Meso-scale features and couple stresses in fracture process zone

Craig N Morrison[1, 3,*], Andrey P Jivkov[2, 3], John R Yates[3]

[1] Nuclear FiRST Doctoral Training Centre
[2] Research Centre for Radwaste and Decommissioning
[3] Modelling and Simulation Centre
Dalton Nuclear Institute, The University of Manchester, Manchester, M13 9PL, UK
* Corresponding author: craig.morrison-2@postgrad.manchester.ac.uk

Abstract Generalized continuum theories such as couple stress theory have the potential to improve our understanding of material deformation and fracture behaviour in areas where classical continuum theory breaks down at, for example, the length scale of meso-scale features within the fracture process zone. The couple stress theory considers not only relative displacements between these features but also relative rotations, introducing a natural length scale. A model has been developed of a low stiffness matrix containing suitably situated high stiffness particles to simulate the presence of defects at the meso-scale. This has been used to assess the descriptive potential of a novel consistent couple stress theory. The model has been subjected to a set of displacement fields selected to produce strain energies with varying contributions from the coupled stresses. The results demonstrate the effect of particle size to spacing ratio on the elastic energies. These can be used to evaluate the couple stress constant as well as validate the constant experimentally for specific materials.

Keywords: generalized continuum; meso-scale defects; FE analysis; strain-curvature energy; size effect

1. Introduction

Analysis of materials at engineering length scales is based upon assumptions of classical continuum behaviour. This is adequate for most macro-scale analyses but, when considering smaller length scales where cracks, notches and defects introduce stress concentrations, the material microstructure is known to have a significant impact on material behaviour [1]. Local approaches, which incorporate mechanistic understanding of material failure behaviour at the length scale of their relevant features, are beneficial for linking microstructures to macroscopic responses [2]. However, the widely used weakest link (WL) assumption has been challenged as a realistic method of modelling size effects in cleavage [3] and quasi-brittle fracture [4] as a result of failing to account for the interaction processes during failure.

Discrete methods have shown promise for modelling materials undergoing such fracture. Lattice models consist of nodes connected into a lattice via springs [5], beams [6] or other discrete elements with the properties of these connections allowing a micro structurally informed response. Lattice modelling differs in principle from previous local approach models by using a statistically parallel system, where loads are redistributed upon the breaking of a single bond, rather than the ultimate failure seen in WL systems. This is considered to be a closer representation of the interaction and coalescence of micro-cracks and flaws, which characterize quasi-brittle materials such as graphite [7] and cement-based materials [8]. The work presented here explores aspects of the site-bond model developed by Jivkov and Yates [9] and used for studies of damage evolution from distributed porosity in cements [10]. Work on this model has shown that evaluating the stiffness coefficients of the bonds using strain energy equivalence between the discrete model and a classical continuum creates an indeterminate problem. Use of a generalized continuum theory, such as couple stress theory, offers a possible solution to this indeterminacy.

In couple stress theory (CST) each point within the continuum has three additional degrees of freedom, point rotations. These are associated with couple stresses as the classical (force) stresses are associated with strains. A general CST was proposed early in the 20th century by the Cosserat brothers [11]. It went largely unnoticed until the 1960s when a desire to understand the mechanisms behind micro-crack growth for more accurate crack assessment rejuvenated interest. One branch of CSTs considers point micro-rotations to be independent of the macro-rotations; the rotations derived from the displacement gradient [12, 13]. These are known as micropolar theories or Cosserat models with free rotations [14]. While such a view appears to be well suited for use with discrete lattice methods, it is difficult to establish a link between a continuum and a discrete representation of a material containing features that are following the deformations of the bulk. For such situations it is more plausible to assume that the micro-rotations are equal to the macro-rotation. This assumption led to a branch of CSTs known as Cosserat models with constrained rotations [14, 15]. Initially, these were based on couple stresses work-conjugate to the macro-rotation gradient. As a consequence, the spherical part of the couple stress tensor remained undetermined. Recently, Hadjesfandiari and Dargush [16] proposed a consistent CST using true kinematic quantities to remove the indeterminacy of the couple stress tensor.

The consistent CST [16] naturally introduces a length parameter. This is of key importance for the local material behaviour. But the calibration of the CST requires that the length parameter is physically related to the material microstructure; the sizes and distances between characteristic features that disturb the symmetry of the stresses. We report on work in progress investigating whether a medium with features can be used to calculate bond responses to bending and torsion in the discrete model [9] and if this can be used to calibrate the consistent CST.

2. Theory and model

2.1 Generalised continuum

The kinematics of a material point under small deformation is given by the displacement gradient, Eq. (1), where comma denotes differentiation, rounded parenthesis denotes symmetric part and square parenthesis denotes skew symmetric part of the tensor. The symmetric (strain tensor e_{ij}) and the skew symmetric (rotation tensor ω_{ij}) parts are given by Eq. (2) and Eq. (3), respectively. The right hand side of Eq. **Error! Reference source not found.** gives the rotation tensor as a vector using the permutation tensor.

$$u_{i,j} = u_{(i,j)} + u_{[i,j]} \tag{1}$$

$$u_{(i,j)} = e_{ij} = \frac{1}{2}\left(u_{i,j} + u_{j,i}\right) \tag{2}$$

$$u_{[i,j]} = \omega_{ij} = \frac{1}{2}\left(u_{i,j} - u_{j,i}\right) = \epsilon_{jik}\omega_k \tag{3}$$

In classical continuum mechanics, the elastic potential depends solely on the strain tensor. In generalised continuum, additional potential is carried by the gradient of the rotation vector, Eq. (4). The symmetric part of this gradient, χ_{ij} in Eq. (5), represent “pure” twists, and the skew symmetric part, κ_{ij} in Eq. (6), represent “pure” curvatures, which can be given by a vector as shown with the right-hand size.

$$\omega_{i,j} = \omega_{(i,j)} + \omega_{[i,j]} \tag{4}$$

$$\omega_{(i,j)} = \chi_{ij} = \frac{1}{2}\left(\omega_{i,j} + \omega_{j,i}\right) \tag{5}$$

$$\omega_{[i,j]} = \kappa_{ij} = \frac{1}{2}\left(\omega_{i,j} - \omega_{j,i}\right) = \epsilon_{jik}\kappa_k \tag{6}$$

Generally, the energy potential of the rotation gradient leads to a non-symmetric force stress tensor, σ_{ji}, Eq. (7), and the introduction of a couple stress tensor, μ_{ji}, Eq. (8). When the force stress is taken as work conjugate to the strain tensor, and the couple stress is taken as work conjugate to the gradient of the rotation, the symmetric part of the couple stress tensor becomes indeterminate.

$$\sigma_{ji} = \sigma_{(ji)} + \sigma_{[ji]} \tag{7}$$

$$\mu_{ji} = \mu_{(ji)} + \mu_{[ji]} \tag{8}$$

Hadjesfandiari and Dargush [16] suggested a solution to this problem by demonstrating that the entire rotation gradient does not have energy potential, only the curvature tensor, Eq. (6). Thus the deformation energy consists of the work done by the force stress on the strain and the work done by the couple stress on the pure curvature. The symmetric part of the rotation gradient, Eq. (5), has no forces associated with it, which solves the problem of the indeterminate spherical part of the rotation gradient. For an isotropic material, the elastic potential is given by [16]:

$$W(\varepsilon,\kappa) = \frac{1}{2}\lambda\,(\varepsilon_{kk})^2 + \mu\,\varepsilon_{ij}\varepsilon_{ij} + 8\eta\,\kappa_i\kappa_i \tag{9}$$

where λ and μ are Lamé parameters and η is a material couple stress constant.

According to this theory, a homogeneous displacement field, such as hydrostatic compression Eq. (10), does not introduce rotations and hence curvatures.

$$u_1 = x_1 \qquad u_2 = x_2 \qquad u_3 = x_3 \tag{10}$$

A displacement field producing pure twist, Eq. (11), introduces rotations, Eq. (12), but no true curvatures[16]:

$$u_1 = -\theta x_2 x_3 \qquad u_2 = \theta x_1 x_3 \qquad u_3 = 0 \tag{11}$$

$$\omega_1 = -\frac{1}{2}\theta x_1 \qquad \omega_2 = -\frac{1}{2}\theta x_2 \qquad \omega_3 = \theta x_3 \tag{12}$$

A displacement field corresponding to pure bending of a beam, Eq. (13), introduces non-zero rotations, Eq. (14), that result in a single non-zero curvature, Eq. (15), [16]:

$$u_1 = -\frac{1}{R}x_1 x_3 \qquad u_2 = -\frac{\nu}{R}x_2 x_3 \qquad u_3 = \frac{\nu}{2R}\left({x_2}^2 - {x_3}^2\right) - \frac{1}{2R}{x_1}^2 \tag{13}$$

$$\omega_1 = \frac{\nu x_2}{R} \qquad \omega_2 = \frac{x_1}{R} \tag{14}$$

$$\kappa_3 = \frac{1-\nu}{2R} \tag{15}$$

where ν is Poisson's ratio and R is the radius of curvature of the beam central axis.

2.2 Discrete site-bond model

The site-bond model [9] uses a discrete lattice, based on a regular tessellation of material space into truncated octahedral cells, Fig. 1(a). The lattice derives from the cellular structure when material particles, attached to cell centres, interact via deformable bonds. The bond properties relate to their ability to transfer shear and axial forces as well as torsion and bending moments to satisfy the six degrees of freedom of each site. A site requires 14 bonds to connect it to its neighbours, Fig. 1(b): six bonds of length $2L$ ($2L$ is the cell size) in principal directions (through square faces), and eight bonds of length $\sqrt{3}L$ in octahedral directions (through hexagonal faces). Development of this model involves bond representations with six independent elastic springs resisting three relative

displacements and three relative rotations between sites. This yields four spring types with axial, K_n, shear, K_s, twisting, K_t, and bending, K_b, stiffness [17], which could, in general, be different for principal and octahedral directions.

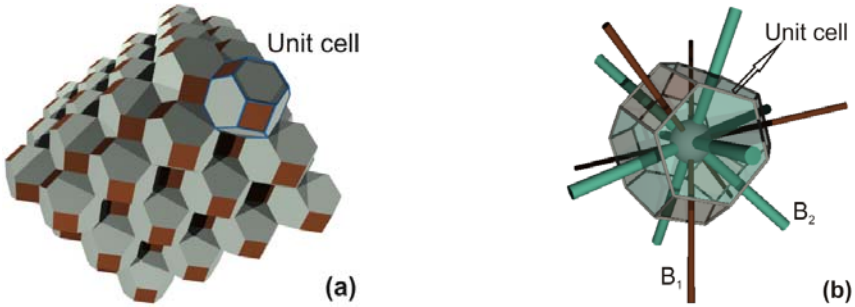

Figure 1. Cellular representation of material (a); and unit cell with bonds (b).

2.3 FE model of elastic continuum with rigid particles

For our investigation, we use a finite element model of a cube of an elastic material surrounding a truncated octahedral cell of size $2L$. The material has a unit modulus of elasticity and Poisson's ratio $\nu = 0.375$. Rigid cubic particles are introduced in the cube, so that one particle, P0, is positioned in the centre of the cell, while others are positioned outside the cell in the principal and octahedral directions as shown in Fig. 2. Three different loading conditions are used: (H) hydrostatic compression; (T) pure twist; and (B) pure bending. These are applied via displacement fields on the cube surfaces; examples for pure twist and pure bending are given in Fig. 3. In all cases we calculate elastic energies, Ω, within the unit cell surrounding the central particle. With no particles present, the cell elastic energy is given by the classical continuum solution, since no features exist to disturb stress symmetry. The displacement magnitudes for the three loading cases are selected so that Ω without particles is the same, Ω_0.

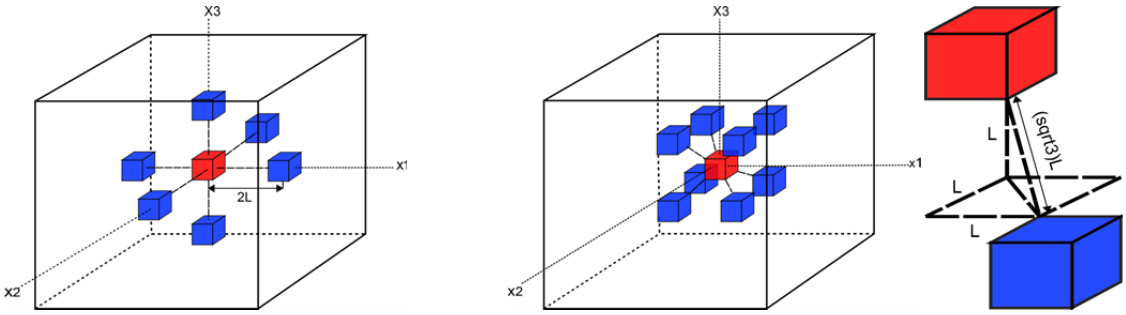

Figure 2. Particle additions in the principal (left) and octahedral (right) directions.

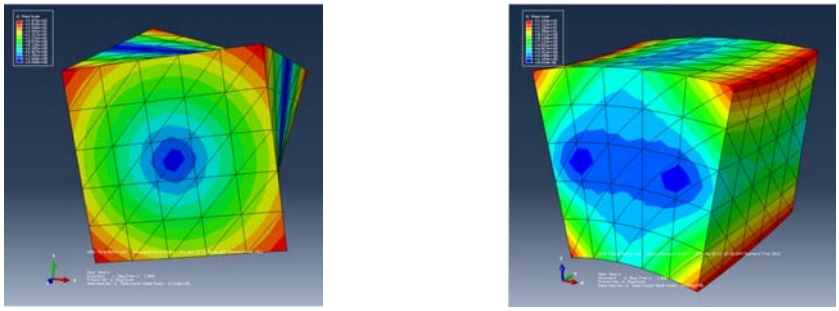

Figure 3. Displacement maps for the loading cases of pure twist (left) and pure bending (right).

To link the cell energies to kinematic quantities we calculate particle translations and rotations using three unit vectors, $\mathbf{n}_1$, $\mathbf{n}_2$ and $\mathbf{n}_3$ normal to three orthogonal faces of a particle, see Fig. 4. After deformation these vectors remain orthogonal as the particles are rigid, given with $\mathbf{t}_1$, $\mathbf{t}_2$ and $\mathbf{t}_3$ in Fig. 4. The coordinates of these, arranged in columns, form the transformation matrix, $\mathbf{T}$, for the particle. The particle motion can be represented by a single rotation, θ given by Eq. (16), around a normalized axis, α given by Eq. (17). The components of the rotation vector for a particle are calculated by Eq. (18). The relative rotations between central and any other particle are expressed in the coordinate system defined by the particular pair using the corresponding transformation.

$$\theta = cos^{-1}\left(\frac{trace\,(\mathbf{T})-1}{2}\right) \tag{16}$$

$$\alpha = \frac{1}{2\sin(\theta)}\begin{bmatrix} T_{32}-T_{23} \\ T_{13}-T_{31} \\ T_{21}-T_{12} \end{bmatrix} \tag{17}$$

$$\omega_i = \theta \times \alpha_i, \quad i = 1,2,3 \tag{18}$$

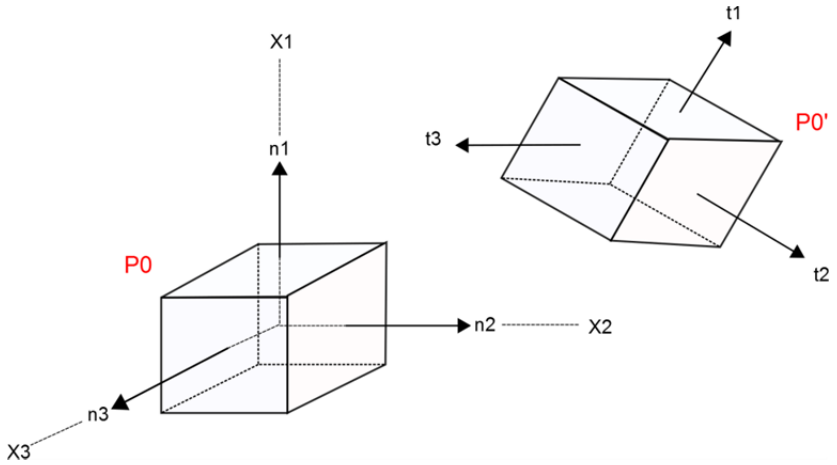

Figure 4. Orthogonal vectors, ($\mathbf{n}_1$, $\mathbf{n}_2$, $\mathbf{n}_3$) and ($\mathbf{t}_1$, $\mathbf{t}_2$, $\mathbf{t}_3$) describing the orientation of P0 before and after deformation respectively.

3. Results and Discussion

For the particle arrangement used (a central particle and all 14 particles of the site-bond model) we have used four different particle sizes relative to the cell size in order to investigate the effect of cell to particle size ratio, λ. The ratios are 3 (large particles), 4, 6, and 12 (small particles).

In the case of hydrostatic loading no rotations of particles were observed and the relative displacements between P0 and any principal or octahedral particle were only axial, conforming to Eq. (10). In the site-bond model these relative displacements should be resisted by axial springs with stiffness coefficients K_n^p and K_n^o, respectively. The relative axial displacements were found independent of λ, scaling with the applied displacements. The cell energies were found to be dependent on λ, as shown in Figure . For small particles, λ = 12, the cell energy approached Ω_0; the presence of particles has negligible effect. The cell energy and displacements from this case can be used to calibrate a linear combination of K_n^p and K_n^o. Note, that in general this case is not sufficient for calibrating stiffness coefficients separately. However, the particle size effect appears to be very

small, suggesting that the two stiffness coefficients could be assumed equal and given from the continuum solution, following [17] for example.

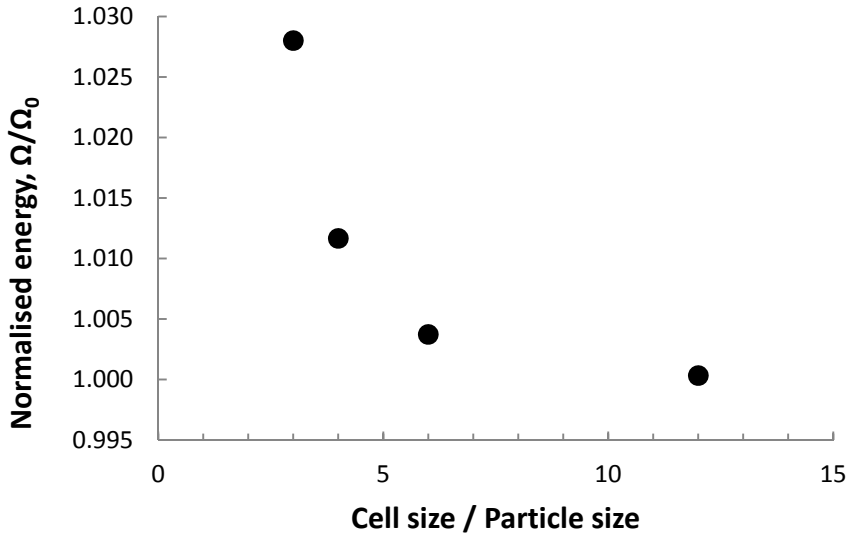

Figure 5. Normalised cell energy vs size ratio under hydrostatic compression.

In the case of pure twist the cell energies were found to be dependent on λ, Fig. 6. While this is similar to the case of hydrostatic compression the effect of particle size is substantially larger. All relative displacements between P0 and the principal particles were zero, conforming to Eq. (11). The relative displacements between P0 and octahedral particles were zero axial and non-zero transversal, again conforming to Eq. (11). This means that the only activated linear springs in the site-bond model are the shear springs in octahedral direction with stiffness K_s^o.

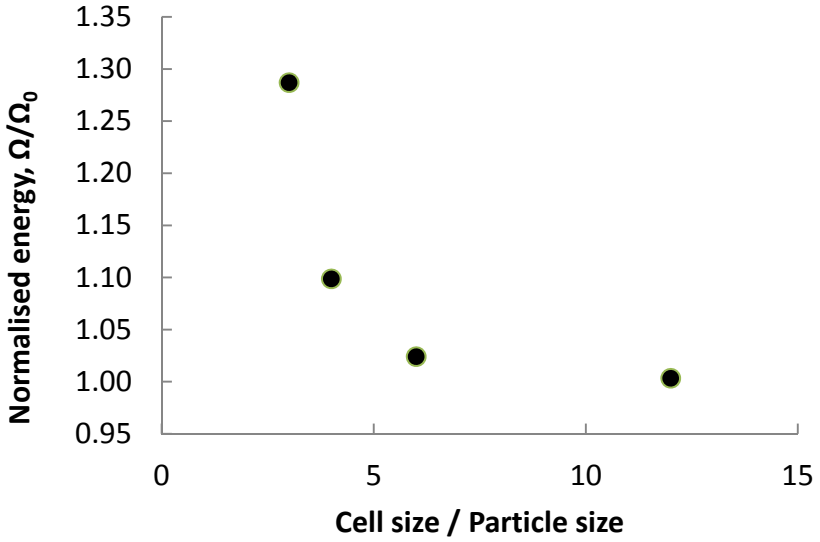

Figure 6. Normalised cell energy vs size ratio under pure twist

The calculated relative rotations between P0 and the particles in the two directions are shown in Fig.

7. The non-zero relative rotations between P0 and principal particles were twists as expected from Eq. (12) and the magnitude shown in Fig. 7 is the twist of the particle in direction X1. It is seen that this is 3-4 orders of magnitude smaller that the relative rotations between P0 and octahedral particles. The latter were found to be bend-type rotations only, conforming to Eq. (12), and suggesting that the only moment springs activated are the bending springs in the octahedral direction with stiffness K_b^o. The magnitudes of the bend-rotations of octahedral particles were found nearly independent of particle size. These results suggest that for the case of pure twist, the elastic strain energy is accumulated in the shear and bending springs in the octahedral direction only, and one can calibrate a linear combination of K_s^o and K_b^o, which should depend on the cell to particle size ratio. From this perspective the results support the analytical derivations in [16], where pure twists do not contribute to the elastic energy. From here, it can be speculated that the torsion springs in the principal directions could be omitted from the site-bond model, i.e. $K_t^p = 0$. This should be supported by considering other cases with curvature-free displacement fields which introduce twists of principal particles according to the theory.

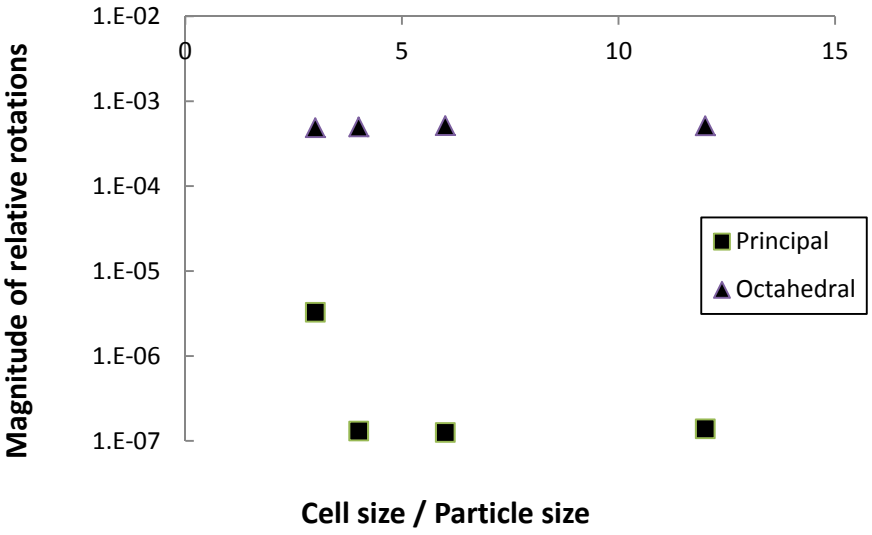

Figure 7. Relative rotation vs size ratio under pure twist

The cell energy dependence on λ for the case of pure bending is shown in Fig. 8. The effect of particle size is smaller than in the case of pure twist, but not negligible. The relative displacements between P0 and the octahedral particles were non-zero axial and tangential, conforming to Eq. (13). The relative displacements between P0 and the principal particles also conform to theory with non-zero axial for particles in X2, non-zero tangential for particles in X1 and zero displacements of particles in X3. This means that the activated linear springs in the site-bond model would be axial and shear springs in all octahedral directions with stiffness coefficients K_n^o and K_s^o, and axial and shear springs in two principal directions with stiffness coefficients K_n^p and K_s^p.

The calculated relative rotations of the particles are shown in Fig. 9. The only non-zero relative rotation of principal particles was found to be the bend-type rotation of the particles in X1, conforming to Eq. (14). However, this relative rotation was found at least an order of magnitude

smaller than the magnitude of the relative rotation between P0 and octahedral particles. The latter contains twist and bend components, suggesting an activation of both the torsion and bending springs in the octahedral direction with stiffness coefficients K_t^o and K_b^o. The much smaller rotation of the principal particles can be used to approximate the kinematics and assume zero rotation of principal particles. Thus the elastic energy is taken by the linear springs in all directions and the torsion and bending spring in the octahedral direction, allowing for calibration of a linear combination of K_n^o, K_s^p, K_n^o, K_s^o, K_t^o and K_b^o, which should depend on the cell to particle size ratio. As in the case of pure twist it can be speculated that the bending springs in the principal direction can be omitted, i.e. $K_b^p = 0$, but this needs to be supported by considering other displacement fields introducing bend-type rotations of principal particles. It can be further speculated, that the torsion stiffness in the octahedral direction should be zero, i.e. $K_t^o = 0$. This could be deduced from the theoretical requirement that pure twists have no energy potential, but requires further investigation. If these were shown to be true, the bending case would provide a calibration for the linear combination of K_n^o, K_s^p, K_n^o, K_s^o, K_b^o.

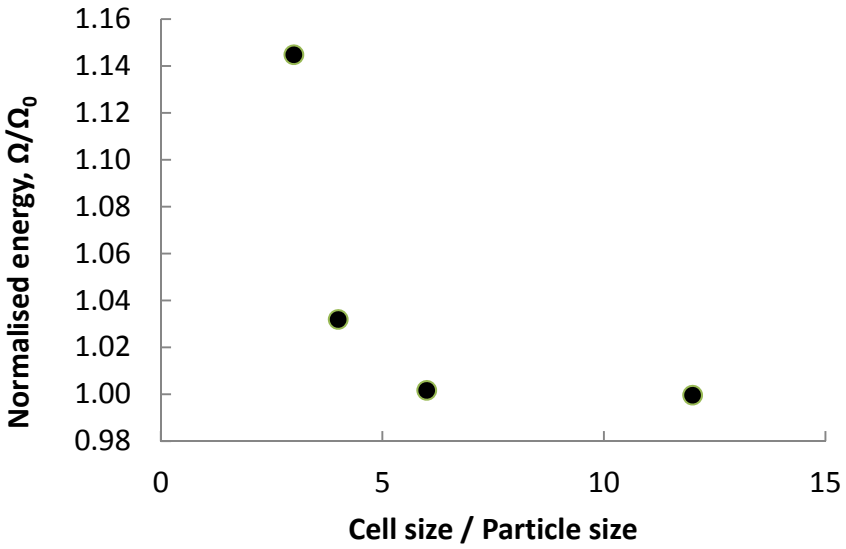

Figure 8 . Normalised cell energy vs size ratio under pure bending

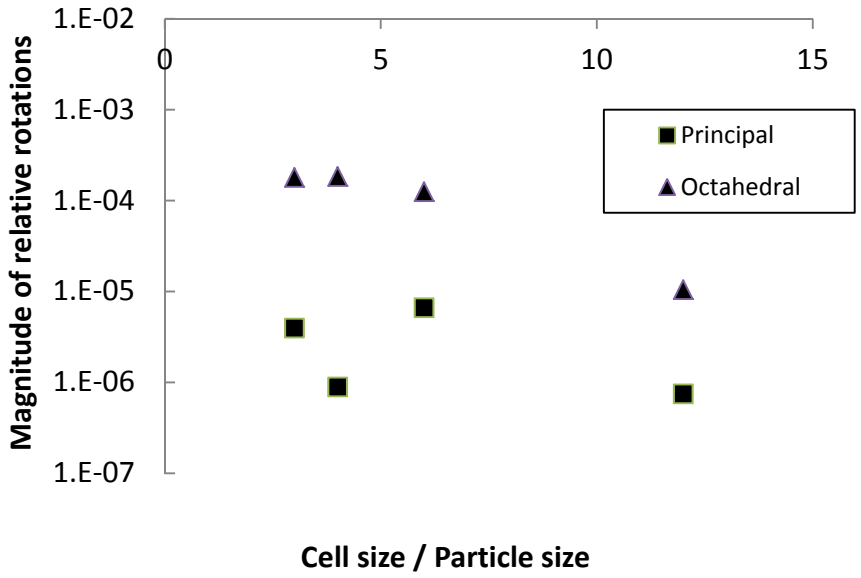

Figure 9. Relative rotation vs size ratio under pure bending

From the three cases considered in this work, it is clear that a separation between all required stiffness coefficients is not possible. However, there is a good indication that the site-bond model should not contain torsion springs and possibly bending springs in the principal directions. One way to check this is pure twist along the octahedral axis, which theoretically should provide twist and bend rotations of all particles. If this proves to be the case, the elastic energy of the continuum with features should be taken by the deformations of the remaining springs. Additional loading cases are necessary to determine the stiffness coefficients of these springs. If these are determined from curvature-free loading cases alone, a good strategy for the calculation of the coupled-stress constant can be proposed. The site-bond model with constants calibrated from curvature-free loading cases can be subjected to a case introducing curvature energy according to theory, for example pure bending, and any excess of energy between the site-bond model and classical continuum should be attributed to curvature energy.

4. Conclusions

- We have proposed a methodology for calibrating the spring constants of a special lattice model using a micromechanical model of a material containing features.
- The comparison of the results with the consistent couple-stress theory suggests that some of the possible moment springs in the lattice could be omitted, reducing the complexity and increasing the correspondence between continuum couple-stress theory and discrete representation.
- We have demonstrated that in all loading cases considered there is an effect of the distance to size ratio of the features, which must be taken into account when calibrating the constants. This suggests that actual microstructure data needs to be used for calibrating the site-bond model.
- The loading cases considered were not sufficient for complete determination of the spring constants of the discrete model. Further work is necessary with loading cases that provide different linear combinations of activated springs' kinematics.

- There is the potential that the lattice model, if fully calibrated with curvature-free loading cases, can provide a means of determining the couple-stress constant for a material with given microstructure properties such as average particle size and distance.

Acknowledgements

The support from EPSRC, via Nuclear FiRST Doctoral Training Centre, to Morrison, from EPSRC via grant EP/J019763/1 and BNFL to Jivkov, and from EDF R+D to Yates is gratefully acknowledged.

References

[1] G.B. Sinclair, A.E. Chambers, Strength size effects and fracture mechanics: What does the physical evidence say? Eng Fract Mech 26 (1987) 279-310.
[2] J. Lemaitre, Local approach of fracture. Eng Fract Mech 23 (1986) 523–537.
[3] A.P. Jivkov, D.P.G. Lidbury, P. James, Assessment of Local Approach Methods for Predicting End-of-Life Toughness of RPV Steels. In Proc. PVP2011 (2011) paper 57546, Baltimore, Maryland.
[4] Z.P. Bažant, S.-D. Pang, Activation energy based extreme value statistics and size effect in brittle and quasibrittle fracture. J Mech Phys Solids 55 (2007) 91–131.
[5] A. Pazdniakou, P.M. Adler, Lattice Spring Models. Transp Porous Med 93 (2012) 243–262.
[6] E. Schlangen, E. Garboczi, Fracture simulations of concrete using lattice models: computational aspects. Eng Fract Mech 57 (1997) 319–332.
[7] N.N. Nemeth, R.L. Bratton, Overview of statistical models of fracture for nonirradiated nuclear-graphite components. Nucl Eng Design 240 (2010) 1–29.
[8] P. Grassl, D. Grégoire, L. Rojas Solano, G. Pijaudier-Cabot, Meso-scale modelling of the size effect on the fracture process zone of concrete. Int J Solids Struct 49 (2012) 1818–1827.
[9] A.P. Jivkov, J.R. Yates, Elastic behaviour of a regular lattice for meso-scale modelling of solids. Int J Solids Struct 49 (2012) 3089–3099.
[10] A.P. Jivkov, M. Gunther, K.P. Travis. Site-bond modelling of porous quasi-brittle media. Mineral Mag 76 (2012) 94-99.
[11] F. Cosserat, E. Cosserat, Theory of Deformable Bodies. A. Hermann et Fils, Paris, 1909.
[12] R.D. Mindlin, Micro-structure in linear elasticity. Arch Ration Mech An 16 (1964) 51–78.
[13] W. Nowacki, Theory of Asymmetric Elasticity. Pergamon Press, Oxford, 1986.
[14] M. Garajeu, E. Soos, Cosserat Models Versus Crack Propagation. Math Mech Solids 8 (2003) 189–218.
[15] R.A. Toupin, Theories of elasticity with couple-stress. Arch Ration Mech An 17 (1964) 85-112.
[16] A.R. Hadjesfandiari, G.F. Dargush, Couple stress theory for solids. Int J Solids Struct 48 (2011) 2496–2510.
[17] Y. Wang, P. Mora, Macroscopic elastic properties of regular lattices. J Mech Phys Solids 56 (2008) 3459–3474.